UCRL-JC-131089
PREPRINT

Investigation of Steady-State and Transient Defect Populations in KH_2PO_4 Subsequent to High Fluence Laser Irradiation

S. G. Demos, M. Staggs, H. B. Radousky, J. J. De Yoreo

This paper was prepared for submittal to the
Photonics West '99 Symposium
San Jose, CA
January 23-29, 1999

January 26, 1999

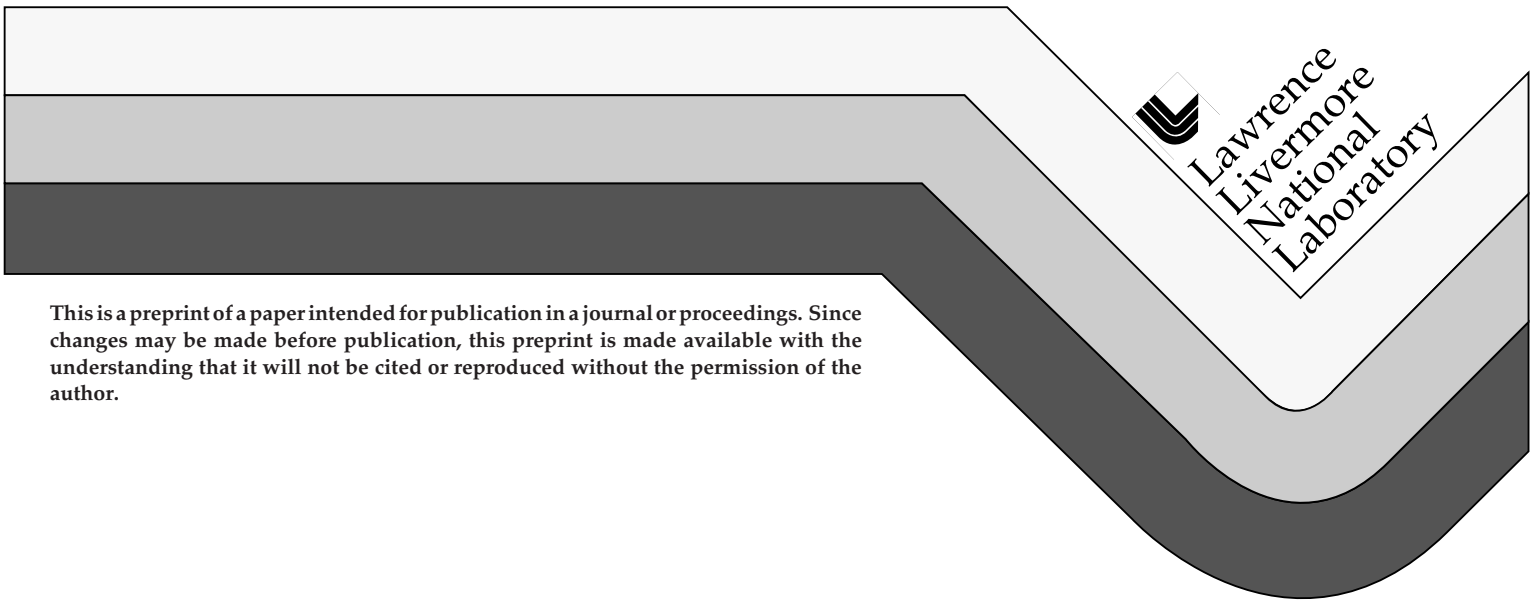

Investigation of steady-state and transient defect populations in KH_2PO_4 subsequent to high fluence laser irradiation

S. G. Demos, M. Staggs, H. B. Radousky and J. J. De Yoreo

Lawrence Livermore National Laboratory, PO Box 808, Livermore, CA 94580.
Tel.: (925) 423 3388, Fax: (925) 423 2463

1. ABSTRACT

Microscopic fluorescence imaging and time-resolved Raman scattering are employed to investigate the effect of high power 355 nm laser irradiation on preexisting and transient defect populations in KH_2PO_4. Defect clusters in the bulk of KDP crystals are imaged with 1 micron spatial resolution using their NIR emission. The intensity of the emission clusters varies widely within the image field. The exposure of the crystal at high power 355 nm, 3 ns laser irradiation leads to a reduction of the number of observed optically active centers. In addition, time resolved Raman scattering was employed to study the transient generation of defects during high power 355 nm laser irradiation.

Key words: KDP, Fluorescence Microscopy, Spectroscopy, Defects, High power lasers**.**

2. INTRODUCTION

Defects are known to greatly influence the fundamental characteristics of many dielectric solid state materials. Uniform distribution of point defects is accompanied under certain conditions by defect aggregation and defect cluster formation. Electronic defects may exist in a crystal lattice in the form of impurity ions or in the form of lattice defects such as interstitial ion vacancies. In many cases, the origin of the defects is the intentional doping of impurity ions in order to introduce novel electronic properties not available to the host crystal. In other cases, the presence of defects is unwanted and may be associated with reduced performance of the material. Defect incorporation into a crystal lattice takes place during growth or subsequently to electromagnetic or particle irradiation. These processes have attracted a great deal of attention in the scientific community due to their importance in processing and performance of materials.

Potassium dihydrogen phosphate (KH_2PO_4, also known as KDP) is a nonlinear optical and electro-optical dielectric crystal that has extensively been incorporated into various laser systems for harmonic generation and electrooptic switching. The ability of KDP to grow at a fast rate, large single crystals (40-55 cm),[1] has made it an important material for large-aperture laser systems. A transient absorption in the 350-700-nm spectral region has been reported when KDP crystals are exposed to intense UV laser irradiation[2,3]. This absorption has been assigned to the formation of transient defect centers.

In this work, defect populations and clusters in the bulk of large KDP crystals are studied using a microscopic fluorescence imaging system. The exposure of the crystal to high power 355 nm, 3 ns laser irradiation leads to a significant conditioning of the KDP, which is correlated with a reduction of the number of observed optically active centers. Spectroscopic measurements reveal the spectral characteristics of the defect population that give rise to the recorded fluorescence images. Pump-probe Raman scattering measurements provide information regarding transient defect population generated during high power laser irradiation.

3. EXPERIMENTAL SET-UP

The experimental layout used in this investigation are shown in figs. 1a and 1b. Fig. 1a depicts the experimental arrangement utilized to obtain microscopic fluorescence images of defect population located inside the bulk of KDP crystals. The third harmonic of a 3-ns pulsewidth, Q-switched, Nd:YAG laser is overlapped with the CW output of an argon laser operating at 514-nm, 488 nm or 351-nm. The two overlapped beams are propagating along the z-axis (optical axis) of the KDP crystal and focused in the bulk of the crystal using a 7.5-cm focal length cylindrical lens. The argon laser was used as the illumination source for the acquisition of the microscopic fluorescence images of the optically active centers. The high-power, 355-nm laser was used for the laser conditioning experiments. The imaging system is positioned along the y-axis of the crystal and perpendicular to the direction of illumination The imaging system is composed of a long working distance microscope objective with magnification power of X20 followed by a X5 magnification zoom lens. The images were recorded using a liquid nitrogen cooled CCD detector. The imaging plane of the microscopic system is overlapped with the focal plane of the cylindrical lens that delivers the illumination beam into the sample. This configuration ensures that an object illuminated by the laser beam is imaged and recorded by the microscopic imaging system. In this arrangement, 1 μm^2 of an

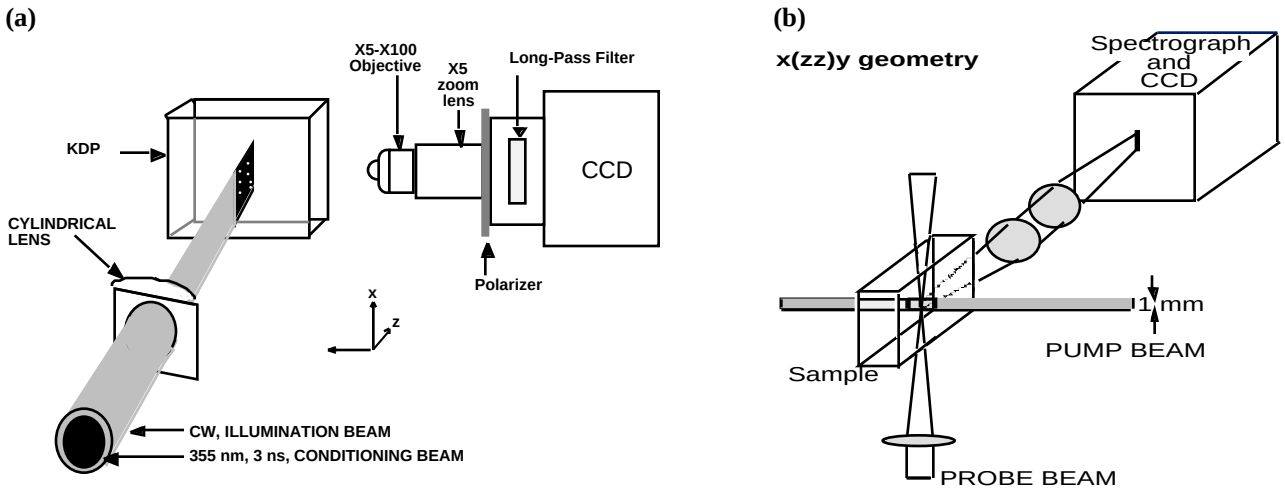

Figure 1. Schematic diagram of the experimental setup (a) microscopic fluorescence imaging system and (b)Pump-probe Raman scattering spectroscopy. Details are provided in the text.

object located at the image plane is projected and recorded on 4 pixels of the CCD. The imaging depth is determined by the ≈ 25 μm width of the illumination slit beam at the focal plane of the cylindrical lens. The polarization vectors of both laser beams are parallel to the x-axis. An analyzer followed by a long-wavelength-pass filter are positioned between the CCD detector and the zoom lens. The analyzer with its polarization vector parallel to the x-axis is used so that the recorded photons have polarization only perpendicular to the optical axis of the crystal and avoid image distortions due to its birefringence. The optical long-wavelength-pass filter is used in order to select for image formation photons from inside the emission band of the optically active centers and discriminate against the Raman scattering signal of the bulk[4] as well as laser light scattered inside the crystal. A 700-nm long-pass (LP) filter was used under 514-nm illumination, a 640-nm LP under 488-nm illumination and, a 520-nm LP under 351-nm illumination.

The experimental arrangement for the Raman scattering experiments is shown in Fig. 1b. The 10 ns, 355 nm third harmonic of the YAG laser is focused to ≈1 mm in diameter and it is used as the pump beam illuminating the sample with ≈5 J/cm^2 along the z-axis of the crystal. The probe laser beam is the 10 ns, 532 nm second harmonic of the YAG laser which illuminates the sample with ≈0.5 J/cm^2 per pulse, with the pump preceding the probe pulses by 10 ns. The probe beam is propagating along the x-axis of the crystal and it is focused to ≈100 μm diameter at the crossing point with the pump beam. The Raman scattering signal from the region of overlap of the pump and probe beams is spectrally analyzed and recorded using a liquid nitrogen cooled CCD detector in the x(zz)y scattering geometry. The samples utilized were conventionally grown and fast grown KDP crystals.[1] The experiments were performed at room temperature.

4. RESULTS

Fig. 2 shows a microscopic fluorescence image of a 200 X 340 X 25 μm^3 section of a fast grown KDP crystal at the sector boundary between the prismatic (material grown on {100} faces) and pyramidal (material grown on {101} faces) sectors. The image was obtained using the X 20 microscope objective under 1.5 Watts, 514 nm, CW laser illumination and a CCD exposure time of 5 minutes. This image shows the presence of emission clusters located inside the bulk of the crystal. The sector boundary is oriented at 45 degrees from the horizontal direction of the image plane with the prismatic sector located in the upper part of the image and the pyramidal sector located in the lower part of the image. This image shows a dramatic difference in the emission cluster concentration within the two crystal sectors which allows for a clear observation of the sector boundary. Although the concentration of the emission clusters is much higher in the prismatic sector, the intensity of individual emission clusters in the two sectors is comparable. In addition to the observation of the emission clusters, a nearly uniform background emission is present that is also different in intensity in the two crystal sectors.

Similar experiment were performed using conventionally grown KDP crystals. The experimental results showed a much lower emission cluster concentration in the conventionally grown crystal than in the fast grown crystal indicating a dependence on the crystal growth method. In addition, the image shown in fig. 2 indicates that within the same crystal, the emission cluster concentration in the prismatic sector is ≈100 times larger than in the pyramidal sector. The overall measured particle concentration is 10^4-10^6 per mm^3 depending on the crystal growth method and crystal sector. Microscopic emission

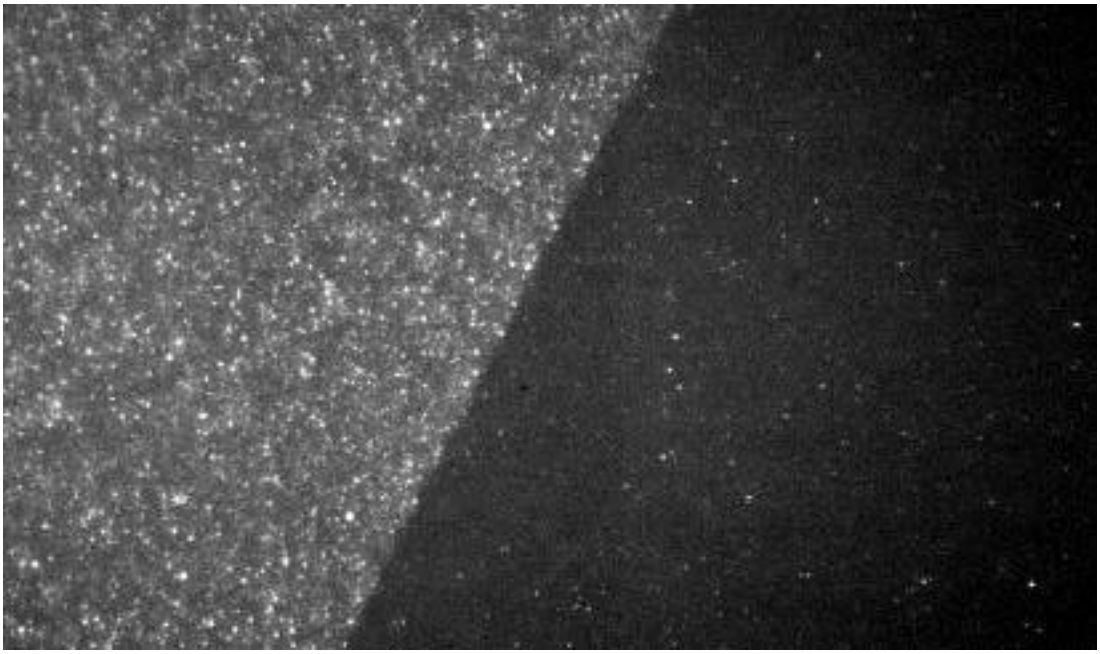

Figure 2. Microscopic fluorescence images from a 200X340X25 μm^3 section of a fast grown KDP crystal at the boundary between prismatic (upper left) and pyramidal (lower right) sectors. Image was obtained using the X20 microscope objective, 514-nm illumination and exposure time of 5 min..

images were also obtained using a X100 magnification microscope objective lens which provided higher resolution images of the defect clusters. The FWHM of the digitized intensity profiles of the observed emission clusters is always nearly 1 μm indicating that this is due to the resolution limit of the imaging system. The actual size of the emission clusters may be much smaller than 1 μm. The experiments were also performed using 488 nm and 351 nm CW laser illumination of avarege power ≈1W and the microscopic fluorescence images were similar to those recorded using 514 nm illumination.

The spectral profiles of the emission from the pyramidal and the prismatic sectors of a fast grown KDP crystal under 351 irradiation were measured at room temperature. Fig. 3a shows that these emission spectra are different in the 450-nm to 800-nm spectral region. This variation gives rise to the differences in the microscopic fluorescence images in the two sectors best

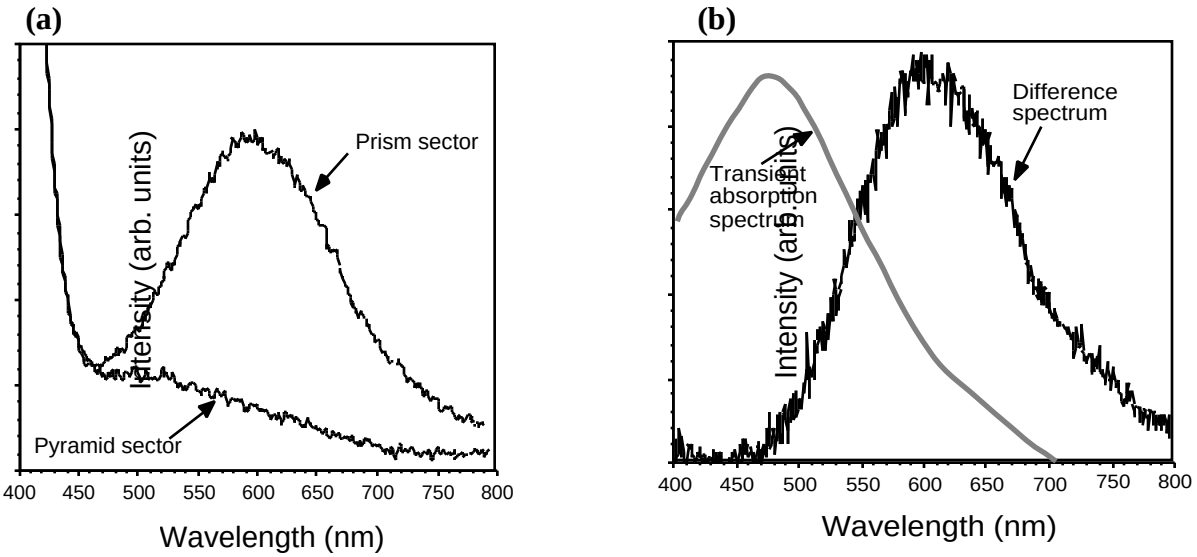

Figure 3. Spectral profiles in the 400 to 800-nm spectral region a) from the prism and pyramid sectors under 351 nm excitation and b) their difference spectrum (the transient absorption spectrum shown is from refs. 2 and 3).

depicted across the sector boundary as demonstrated in fig. 2. An emission band is present in this spectral region in the prismatic sector. In the pyramidal sector, this emission band is much weaker in intensity and appears to be slightly blue-shifted when compared to that of the prism sector. The recorded signal at wavelengths shorter than 450-nm is attributed to Raman scattering. Since the sample is a single crystal, the selection rules for Raman scattering are the same in both crystal sectors and the Raman scattering intensity should be the same. This is in agreement with the spectra shown in fig. 2.

Suppose that the physical nature and thus, the emission profiles of the optically active defects in the two crystal sectors are the same. In this case, subtraction of the emission profiles from the two crystal sectors allows for the extrapolation of the spectral characteristics of these defects. The difference spectrum shown in fig. 3b shows an emission band in the 500-700 nm spectral region. Fig. 3b also contains the transient absorption spectrum measured in refs. X and X for comparison and possible correlation. Discussion on this issue is included in the next section.

Fig. 4a shows the fluorescence image of a 150 X 300 X 25 μm^3 section of the crystal prior to any exposure to high power UV irradiation. The image was obtained using 488 nm CW illumination with the 640 nm long pass filter for wavelength selection and CDD exposure time of 3 minutes. The image shows the presence of emission clusters superimposed to an almost uniform background emission having average intensity of ≈60 counts per CCD pixel. The exact segment of the sample was thereafter exposed to 7 pulses of 3 ns, 355 nm irradiation having average power of ≈5 J/cm^2. The damage threshold in this crystal for the same irradiation parameters is ≈ 7 J/cm^2. The subsequent to UV irradiation fluorescence image is shown in fig. 4b. The number of emission clusters observed in this image is significantly smaller to that of the original image showing a conditioning effect. The number of emission clusters is further reduced when the sample was exposed to additional 355 nm pulsed irradiation. This is demonstrated in fig. 4c where the fluorescence image of a section of the sample is shown following 1700 pulses at ≈5 J/cm^2. The number of emission clusters of the images shown in figs. 4a, 4b and, 4c are approximately $3X10^5$, $2X10^5$, and $0.5X10^5$ per mm^3 corresponding to the original cluster concentration, to that following irradiation with 7 UV pulses and 1700 UV pulses, respectively.

The gray-scale intensity in the three images shown in figs. 4a, 4b and 4c is the same allowing for a comparison of the peak intensity of the emission clusters as well as to the intensity of the background emission. These images demonstrate that the conditioning effect is not limited only to the reduction of the number of observed emission clusters but extends to the intensity decrease of the background emission field. The concentrations of the emission clusters and the intensity of the background emission as a function the number of pulses that irradiated the sample are shown in fig. 5a and 5b, respectively. These results indicate that the conditioning effect takes place at a faster pace during initial irradiation with 355 nm pulses and slows down thereafter. This is also indicated by the nearly adequate linear fit of the experimental data in the logarithmic representation of the experimental data shown in figs. 5a and 5b.

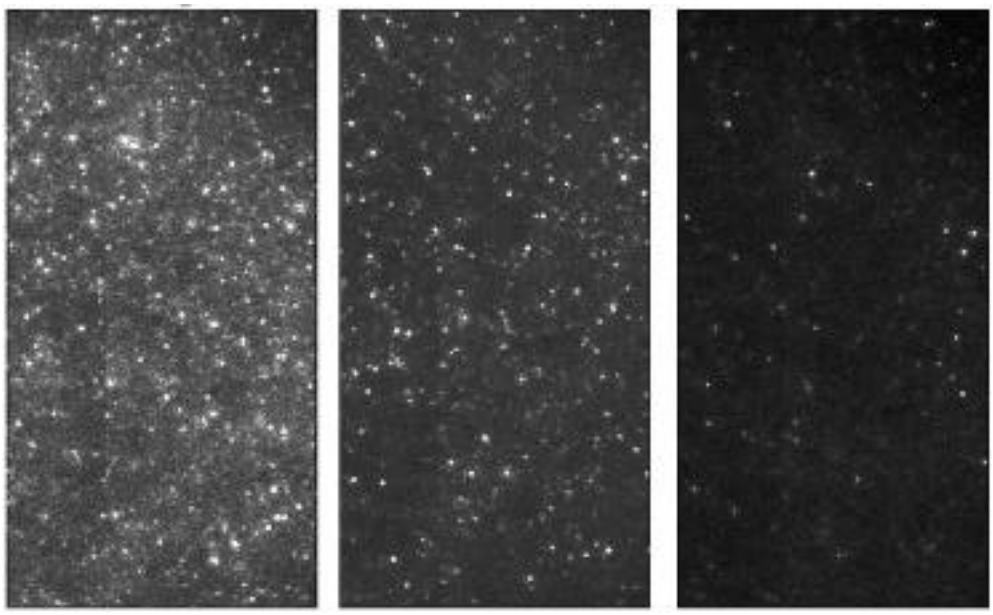

(a) **(b)** **(c)**

Figure 4. A150 X 300 X 25 μm^3 section of the crystal a) prior to any exposure to high power UV irradiation b) following 3 ns, 355 nm, ≈5 J/cm^2 irradiation with 7 pulses c) following irradiation with 1700 pulses.

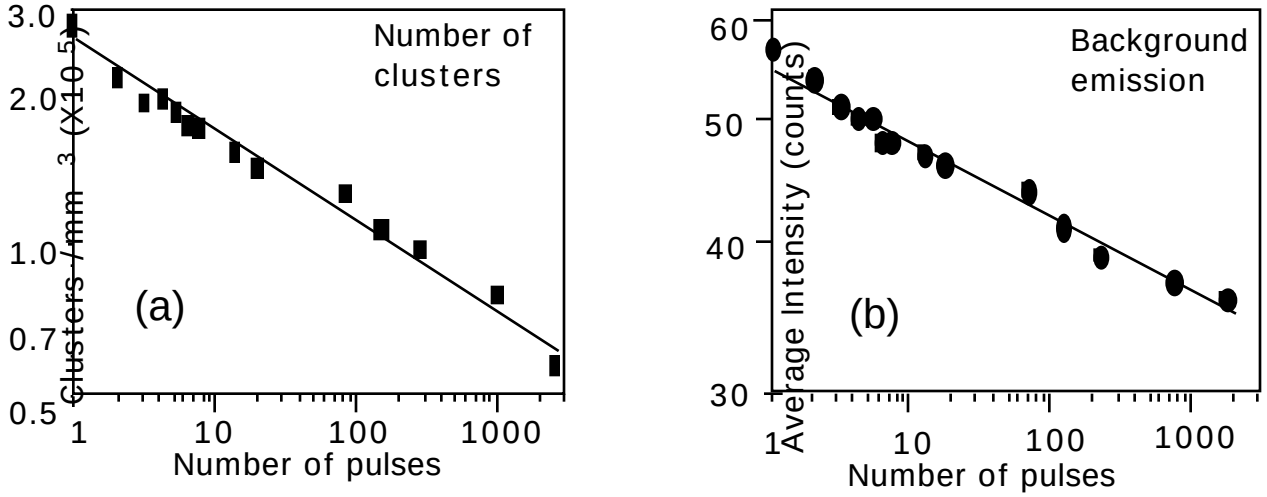

Figure 5. The change of a) the number of emission clusters and b) the intensity of the uniform background emission as a function of the number of high power, 355 nm irradiation pulses.

The conditioning effect depicted in figs. 4 and 5 indicate strong photo-induced process during high power, 355 nm irradiation of the sample. To study these processes, the pump and probe Raman scattering experimental set up shown in fig. 1b was employed. The high-power, 355 nm pump beam irradiated the sample and the Raman scattering spectrum of the 532 nm probe beam was recorded.

Fig. 6 shows the Stokes and anti-Stokes Raman spectra of the 532 nm probe beam when the pump beam is on and when the pump beam is turned off. Three peaks arising from the internal PO_4 vibrational modes are observed in the x(zz)y geometry located at 363 cm^{-1} (ν_2), at 515 cm^{-1} (ν_4) and at 915 cm^{-1} (ν_1).[4] The two spectra are overlapping except for the 915 cm^{-1} peak which has higher intensity (the difference in intensity is denoted as ΔI) when the pump beam is illuminating the sample. The difference in intensity is $\Delta I \approx 0.041\ I_{max}$ where I_{max} is the peak intensity of the 915 cm^{-1} line. The intensity of the anti-Stokes 363 cm^{-1} peak remains the same in both cases which indicate that there is no change of the crystal temperature within the experimental resolution of the Raman scattering system, which is limited to approximately a few degrees K. The same conclusion is reached when the ratio of the Stokes over the antiStokes intensities of the 915 cm^{-1} modes is used to obtain information regarding the temperature of the sample at the point where the pump and probe beams are overlapping.

The experiment was also performed using the 514 nm, CW output of the Argon laser as the probe beam. In this case, the Raman scattering spectra of the probe beam when the high power 355 nm laser pulses were illuminating the sample were identical, within our experimental resolution, to the Raman scattering spectra obtained with the pump illumination turned off. These results indicate a transient change of the intensity of the 915 cm^{-1} mode following the 10 ns, 355 nm illumination. This change in intensity of the 915 cm^{-1} line is observed in the Raman spectrum obtained under 532 nm pulsed illumination (probe), using a delay time of 10 ns between pump and probe pulses but it is smeared out when the 514 nm, CW beam is used as probe. Taking into account that the repetition rate of the laser is 10 Hz and that the experimental resolution in detecting differences in the intensity of the 915 cm^{-1} Stokes Raman line is approximately 0.1 ΔI (ΔI is the observed change in intensity of the 915 cm^{-1} Raman line under 532 nm pulsed illumination), one concludes that the time duration of the transient change of the intensity of the 915 cm^{-1} modes must be shorter than 10 μs.

5. DISCUSSION

The microscopic fluorescence imaging system utilized in this investigation was designed to provide information regarding the distribution of defect clusters or particles inside a transparent optical material with diffraction limited spatial resolution. The observed discrete emission clusters in the bulk of KDP crystals is accompanied with the presence of an emission background that is not perfectly uniform. The conventionally grown KDP crystals have smaller emission cluster concentrations than the fast grown crystals. In addition, in fast grown crystals, the emission cluster concentration in the pyramidal sector is ≈100 times larger than in the prismatic sector. The overall measured emission cluster concentration is 10^4-10^6 per mm^3 depending on the crystal growth method and crystal sector. It is known that the pyramidal sector has a

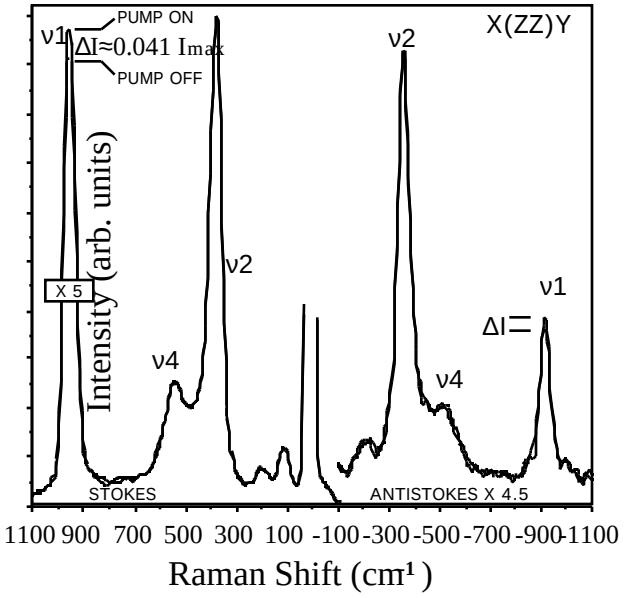

Figure 6. Stokes and anti-Stokes Raman spectra of the 532 nm probe beam when the high fluence 355 nm pump beam is on and when the pump beam is turned off. The intensity of the anti-Stokes Raman spectrum is enhanced by a factor of 4.5. ΔI denotes the change in intensity of the 915 cm^{-1} mode when the pump beam illuminates the sample.

much smaller impurity ion concentration than the prismatic sector due to the difference in the incorporation of impurities into the crystal during growth.[5] The density of the emission clusters in the fast grown KDP crystals observed in this work is $\rho_{em.clu.} \approx 10^6/mm^3$ while the impurity ion density in the prismatic sector is on the order of $\rho_{KDP} \approx 10^{14}/mm^3$. This indicates that the observed clusters do not arise from individual impurity ions although it is known that impurity ions promote the formation and aggregation of defects. It is reasonable to assume that the observed emission clusters arise from foreign particles or most likely defect clusters in the bulk of the crystal. Uniformly distributed impurity ions or defects should contribute in the observed emission background.

The investigation of the reduction of the number of emission clusters under high power 355-nm irradiation shown in fig. 5 indicated that this process takes place at a faster rate at the beginning exhibiting a nearly logarithmic dependence on the number the 355-nm "conditioning" pulses. In addition to the decrease of the number of emission clusters, the intensity of the uniform background of the microscopic fluorescence images also decreases under exposure to high power 355-nm irradiation indicating the presence of "unclustered" defect centers in the material. Supplementary experiments have indicated that the rate of conditioning depends on the energy of the "conditioning" 355 nm pulses.

The Raman scattering experiment manifest an increase of the intensity of the 915 cm^{-1} mode when the 355 nm illumination beam is present which may be attributed to the following possibilities: 1) the presence of stress causing change of the Raman spectrum, 2) depolarization of the Raman scattering light causing spectral components other than the A1 modes being observed and, 3) change of the absorption characteristics following the pump pulse causing resonant Raman enhancement. Past work has demonstrated that when stress is applied in KDP crystals, shifting of the position of individual Raman scattering modes is observed.[6] In this experiment, no shifting of the modes is observed within the experimental resolution of the system (≈8 cm^{-1}). If the cause of the observed changes is laser induced depolarization, one would expect that in addition to the A_1 modes observed in the x(zz)y geometry, the spectral characteristics of the Raman spectrum in the x(zx)y geometry (the main feature of this spectrum is a broad line centered at ≈525 cm^{-1}) should become more prominent. However, this does not happen. No alteration other than the intensity change of the 915 cm^{-1} line in the x(zz)y Raman spectrum is observed when the 355 nm pulses illuminate the sample. In addition, depolarization will lower the intensity of all A1 modes rather than increasing the intensity of only one of these modes. A transient change of the absorption might be another reason for the observed changes. Absorption can be due to impurity ions (X) replacing P in tetrahedrally coordinated sites. Due to resonant enhancement, Raman scattering lines associated with local modes of the XO_4 may be observed. However, due to the difference in mass between the impurity ion X and the ions P that it replaces, the local modes should be shifted in energy with respect to the PO_4 internal modes.[7] This is not consistent with the experimental observations. The above discussion indicates that if absorption is the source of the changes in the Raman spectrum, it has to be associated with the PO_4 itself. In this case, the internal modes of PO_4 that should be most enhanced are the totally symmetric ones[8] and foremost, the tetrahedral 915 cm^{-1} breathing mode which is the only totally symmetric mode in the C_2 site symmetry that originates in a

totally symmetric representation in the T_d molecular symmetry. This model is consistent with the experimental results, where the 915 cm^{-1} mode is enhanced without any shifting in energy.

The changes observed using the pump-and-probe experimental technique employed in this work are associated with the presence of photoexcited species and subsequent transient changes of the absorption characteristics of the material. Recently it was reported that intense 355-nm or 266-nm laser irradiation of KDP crystals at room temperature leads to the formation of a broad transient optical absorption band in the 300-nm to 650-nm spectral region.[2,3] This spectrum is shown in fig. 3b. This laser induced transient absorption was assigned to the formation of $(HPO_4)^-$ centers that are initiated by multi-photon absorption followed by the transport of a hydrogen atom.[2] This hypothesis is supported by the Raman scattering experimental results which indicate the direct involvement of the PO_4 tetrahedron. The 532 nm probe beam used in the Raman scattering experiment is in energy resonance with the transient absorption spectrum and hence, resonance Raman scattering enhancement arising from the transient defect population is possible. The experimental techniques employed in this work do not allow for a positive identification of the defects responsible for the fluorescence images obtained. However, the spectral profile of the difference spectrum shown in fig. 3b may be interpreted as the red-shifted emission arising from defect formations similar or identical to those that give rise to the transient absorption spectra under high-power laser illumination suggesting the presence of $(HPO_4)^-$ defect clusters. It must be pointed out that the crystals studied were not exposed to any prior laser or other type of irradiation.

The experimental results reveal the presence of a steady state defect population preexisting to any irradiation of the sample and a transient defect population generated during high power laser irradiation. The conditioning effect of the preexisting defects taking place during 355 nm irradiation may suggest interaction between the transient defect population with the steady-state defects. The result of this interaction is the reduction of the overall defect population by some defect recombination process. Another scenario might be that the two defect populations do not interact and that the conditioning effect is the result of photophysical processes associated with intense absorption of the laser light by the defect clusters. Our experimental results do not provide a clear answer to the possible laser conditioning mechanisms nor on the makeup of the observed emission clusters. However, one may notice the symmetry in the spectral domain in the transient absorption spectrum and the emission spectrum of the steady-state defects shown in fig. 3b suggesting fundamental similarities in the two defect populations.

6. CONCLUSION

In conclusion, investigation of KDP crystals using microscopic fluorescence imaging revealed the presence of optically active defect clusters located in the bulk of the crystal. The observed defect cluster concentration varies between 10^4-10^6 per mm^3 depending on the crystal growth method and sector of the crystal. Exposure of the crystal to high power, 355-nm, 3-ns, laser irradiation results in the reduction of the number of observed emission clusters. The spectroscopic measurements indicate that the absorption band of these defects is at photon energies higher than 2 eV. Pump-and-probe Raman scattering experiments strongly suggests of transient change of the absorption with direct involvement of the PO_4 tetrahedron.

7. ACKNOWLEDGMENTS

This work was supported under the auspices of the U.S. Department of Energy by the Lawrence Livermore National Laboratory under contract N0. W-7405-ENG-48 through the Institute for Laser Science and Applications.

8. REFERENCES

1. N. P. Zaitseva, J. J. De Yoreo, M. R. Dehaven, R. L. Vital, K. E. Montgomery, M. Richardson, and L. J. Atherton, Rapid growth of large-scale (40-55 cm) KH_2PO_4 crystals, J. Crystal Growth, **180**, 255 (1997).
2. J. E. Davis, R. S. Hughes Jr. and H. W. H. Lee, Investigation of optically generated transient electronic defects and protonic transport in hydrogen-bonded molecular solids - isomorphs of KH_2PO_4, Chem. Phys. Lett. **207**, 540 (1993).
3. C. D. Marshall, S. A. Payne, M. A. Henesian, J. A. Speth, and H. T. Powell, ultraviolet-induced transient absorption in potassium dihydrogen phosphate and its influence on frequency conversion, J. Opt. Soc. Am. B, **11**, 774 (1994).6. C. Y. She, T. W. Broberg and David F. Edwards, Raman Spectra of KH_2PO_4, Phys. Rev. B, **4**, 1580, (1971).
4. C. Y. She, T. W. Broberg and D. F. Edwards, Raman Spectra of Tetragonal KH_2PO_4, Phys. Rev. B, **4**, 1580, (1971).
5. M. Yan, R. Torres, M. Runkel, B. Woods, I. Hutcheon, N. Zaisteva and J. J. DeYoreo, SPIE, **2966**, 11, (1996).
6. I. Tenenaka Y. Tominaga, S. Endo and M. Kobayashi, High Pressure Raman Scattering and Local Distortion of PO_4 in paraelectric KH_2PO_4, Solid State Commun. **84**, 931, (1992).
7. Dana M. Calistru, S. G. Demos and R.R. Alfano, "Anharmonic Effects and Second-Neighbor Interaction of Local Modes in Cr^{4+}-doped Forsterite Probed by Higher Order Resonance Raman Scattering", Phys. Rev. B, **52**, 15253, (1995).
8. A. C. Albrecht, On the Theory of Raman Intensities, J. Chem. Phys., **34**, 1476 (1961)